



HAL
open science

A High Power Buckypaper Biofuel Cell: Exploiting 1,10-Phenanthroline-5,6-dione with FAD-Dependent Dehydrogenase for Catalytically-Powerful Glucose Oxidation

Andrew J. Gross, Xiaohong Chen, Fabien Giroud, Caroline Abreu, Alan Le Goff, Michael Holzinger, Serge Cosnier

► **To cite this version:**

Andrew J. Gross, Xiaohong Chen, Fabien Giroud, Caroline Abreu, Alan Le Goff, et al.. A High Power Buckypaper Biofuel Cell: Exploiting 1,10-Phenanthroline-5,6-dione with FAD-Dependent Dehydrogenase for Catalytically-Powerful Glucose Oxidation. *ACS Catalysis*, 2017, 7 (7), pp.4408 - 4416. 10.1021/acscatal.7b00738 . hal-01616374

HAL Id: hal-01616374

<https://hal.univ-grenoble-alpes.fr/hal-01616374>

Submitted on 19 Nov 2020

HAL is a multi-disciplinary open access archive for the deposit and dissemination of scientific research documents, whether they are published or not. The documents may come from teaching and research institutions in France or abroad, or from public or private research centers.

L'archive ouverte pluridisciplinaire **HAL**, est destinée au dépôt et à la diffusion de documents scientifiques de niveau recherche, publiés ou non, émanant des établissements d'enseignement et de recherche français ou étrangers, des laboratoires publics ou privés.

A High Power Buckypaper Biofuel Cell: Exploiting 1,10-Phenanthroline-5,6-dione with FAD-Dependent Dehydrogenase for Catalytically-Powerful Glucose Oxidation

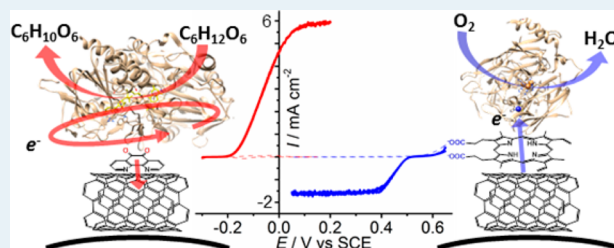
Andrew J. Gross,^{*} Xiaohong Chen,[†] Fabien Giroud, Caroline Abreu, Alan Le Goff,[†] Michael Holzinger,[†] and Serge Cosnier^{*}

Department of Molecular Chemistry, UMR CNRS-UGA 5250, Université Grenoble Alpes, 38000 Grenoble, France

S Supporting Information

ABSTRACT: Enzymatic biofuel cells generate electrical energy from renewable sources with high selectivity and environmental benefits compared to lithium batteries and traditional fuel cells. For enzymatic fuel cells to become competitive, major improvements in electrode design are required to enhance power density, voltage output, and stability. Here we have developed a freestanding paper biofuel cell comprising redox molecule embedded multiwalled carbon nanotube papers for electrical wiring of enzymes. The drop-coat and one-pot fabrication methods provide flexibility and permit easy scalability of functionalized bioelectrodes via commercially available materials. Buckypaper functionalized with 1,10-phenanthroline-5,6-dione (PLQ) as an efficient electron mediator for fungal-derived FAD-dependent glucose dehydrogenase (FADGDH) shows very high steady-state current densities for glucose oxidation of $I_{\max} = 5.38 \pm 0.54 \text{ mA cm}^{-2}$ at 0.15 V vs SCE at neutral pH. When coupled with a bioinspired protoporphyrin IX buckypaper cathode, the resulting glucose/ O_2 fuel cell delivered a power density of $0.65 \pm 0.1 \text{ mW cm}^{-2}$ or $24.1 \pm 4.7 \text{ mW cm}^{-3}$ at a cell voltage of 0.5 V, limited by the cathode. Galvanostatic and current discharge experiments confirm robust short-term operational performance.

KEYWORDS: bioelectrocatalysis, biocatalyst, paper electrode, enzymatic, FAD-GDH, multicopper oxidases



INTRODUCTION

Enzymatic biofuels (EBFCs) convert chemical energy into electrical energy under mild conditions from the oxidation of organic fuels such as sugars and alcohols, coupled with the reduction of oxygen using redox enzymes as bioelectrocatalysts.^{1–3} Biofuel cells offer several advantages over lithium batteries and traditional fuel cells, including the use of renewable, low-cost, and safe fuels from ecological sources and operation at neutral pH and ambient temperature. Furthermore, EBFCs can operate as membraneless fuel cells owing to the high selectivity of enzymes. Particular attention of biofuel cells over the past decade has been directed toward the use of EBFCs as micropower sources which harvest energy from biological fluids for implantable medical devices.^{4–7} In recent years, EBFCs have been successfully implanted in rats,⁴ lobsters,⁵ and snails.⁶ Application of EBFCs for portable and wearable devices is more feasible and has enormous potential. For example, epidermal and contact-lens biofuel cells which harvest energy from sweat or tears using carbon nanotube based electrodes have started to emerge.^{8–10} Lightweight biofuel cells with small form factors offer the prospect of self-powered chemical sensors with in situ detection and remediation of toxic chemicals.^{11,12}

Specific challenges in EBFC electrode design include the development of electrodes which offer (i) stable immobilization of enzymes and mediators with high loadings, (ii) efficient

electron transfer between the active sites of enzymes and the electrode, and (iii) fast mass transport and (iv) are lightweight and easily integrated into devices. To achieve the practical application of biofuel cells, a rapidly emerging approach is to use flavin adenine dinucleotide-dependent glucose dehydrogenase (FADGDH) for catalytic oxidation of glucose at the anode. The FADGDH enzyme offers major advantages for biofuel cells compared to other popular FAD-dependent enzymes such as the gold standard glucose oxidase (GOx).^{13,14} Unlike GOx, FADGDH is oxygen insensitive, which prevents consumption of valuable oxygen at the anode. In situ production of hydrogen peroxide, which can be toxic to single compartment fuel cells, is also avoided.¹⁴ However, the commercially available fungal FADGDH does not have the cytochrome-complex subunit for direct electron transfer (DET) with electrodes.¹⁵ As such, the fungal FADGDH requires an artificial electron transfer mediator, which can result in kinetic and thermodynamic losses compared to DET.¹⁶ The identification of high performance mediators is vital for fungal FADGDH for both biofuel cell and sensor applications. Few systems for mediated electron transfer with FADGDH have been investigated and are mainly based on osmium,^{13,17–19} ruthenium,²⁰ and ferro-

Received: March 7, 2017

Revised: May 15, 2017

Published: May 22, 2017

72 cene^{14,21} redox complexes and polymers. These mediators have
73 high redox potentials and slow mediator exchange due to
74 structural rigidity and require complicated synthesis from toxic
75 precursors. Compared to metal-based mediators, small organic
76 mediators with fast mediator exchange are attractive. For
77 example, 1,2 and 1,4 naphthoquinones^{22,23} and phenothia-
78 zines^{24,25} are commonly exploited and give high catalytic
79 currents at attractively low formal redox potentials.

80 Carbon nanotubes (CNTs) offer great advantages for
81 bioelectrodes and are typically deposited onto an electrode
82 support to give a large surface area with good stability and
83 conductivity.²⁶ CNT-supported electrodes tend to be heavy,
84 bulky, and not easily miniaturizable.^{27,28} Free-standing bucky-
85 paper electrodes prepared by vacuum filtration of CNT
86 suspensions on the other hand are thin and lightweight and
87 offer the possibility to immobilize catalysis-promoting aromatic
88 molecules by π -stacking interactions.^{29–32} However, such paper
89 electrodes are often fragile with limited conductivity and slow
90 electron transfer kinetics compared to conventional bulk
91 electrodes such as glassy carbon (GC). Further improvements
92 in fabrication methods are required toward CNT paper
93 electrodes with excellent homogeneity, reproducibility, and
94 electrochemical properties.

95 In this study, we report the preparation of new redox
96 molecule embedded buckypapers for bioelectrocatalysis using
97 four different types of commercially available redox molecules.
98 The focus of the study is the development of high performance
99 catalytic buckypaper bioelectrodes for enzyme wiring without
100 the use of a supporting substrate or polymer scaffold. The use
101 of 1,10-phenanthroline-5,6-dione (PLQ) as a small electron
102 mediator for the fungus-derived FADGDH is explored, and the
103 resulting buckypaper anode integrated into a fully freestanding
104 paper glucose/O₂ biofuel cell with a protoporphyrin bucky-
105 paper cathode. Notably, our approach here uses PLQ as a small
106 organic mediator and nanotube binder and therefore avoids
107 polymer and metal complex synthesis. This is in contrast to the
108 structurally and electronically different Ru polymer mediator
109 with PLQ ligands reported previously.²⁰

110 ■ EXPERIMENTAL SECTION

111 **Materials and Apparatus.** Monosodium phosphate
112 monohydrate (NaH₂PO₄, ≥98%), disodium hydrogen phos-
113 phate heptahydrate (Na₂HPO₄, 98–102%), *N,N*-dimethylfor-
114 mamide (DMF, 99.9%), potassium ferricyanide, 1,10-phenan-
115 throline-5,6-dione (PLQ, 97%), protoporphyrin IX (PP, ≥95%),
116 ferriprotoporphyrin IX (FePP, ≥98.0%), 1,4 naphthoquinone
117 (NQ, 97%), potassium chloride (KCl, 99%), D-(+)-glucose
118 (≥99.5%), sodium citrate (>99%), sodium chloride (NaCl,
119 99.8%), copper chloride (CuCl₂, 97%), hydrogen peroxide
120 (H₂O₂, 30 wt % in H₂O), ethylenediaminetetraacetic acid
121 (EDTA, 99%), and sulfuric acid (95–98%) were purchased
122 from Sigma-Aldrich and used as received. Bilirubin oxidase
123 (BOD, 1.2 U mg⁻¹) from *Myrothecium sp.* and flavin adenine
124 dinucleotide-dependent glucose dehydrogenase (FADGDH,
125 1150 U mg⁻¹ solid) from *Aspergillus sp.* were purchased from
126 Amano (Japan) and Sekisui Diagnostics (UK), respectively, and
127 used as received. Enzymes were stored at -20 °C. Distilled
128 water was obtained by water purification to a resistivity of 15
129 MΩ cm using a Millipore Ultrapure system. Commercial grade
130 multiwalled carbon nanotubes (MWCNTs, Ø = 9.5 nm, 1.5 μm
131 length, ≥95% purity) were obtained from Nanocyl and used as
132 received without purification. High purity oxygen and argon

were obtained from Messer. Glucose solutions were left to
133 mutarotate overnight to β-D-glucose prior to use. 134

Preparation of Unmodified MWCNT Buckypaper and
Redox-Embedded MWCNT Buckypaper Electrodes by
Drop-Coat Method. First, a 1 mg mL⁻¹ MWCNT suspension
137 was prepared by the addition of 150 mg of nonfunctionalized
138 MWCNTs into 150 mL of DMF. The dispersion was then
139 sonicated for 30 min prior to use. After vigorous shaking for 1
140 min, 66 mL of the suspension was filtered through a Millipore
141 PTFE filter (JHWP, 0.45 μm pore size, Ø = 46 mm) using a
142 vacuum pump, washed with distilled water, and left for 1 h.
143 After filtration, the resulting unmodified buckypaper with Ø =
144 35 mm was left to dry at room temperature. The buckypaper
145 was obtained after its careful removal from the filter paper, then
146 cut into individual electrodes with Ø = 10 mm (geometric
147 surface area of 0.785 cm⁻²) using a metal cutter. To obtain
148 functionalized MWCNT buckypaper electrodes, 150 μL of 0.6
149 mmol L⁻¹ or 10 mmol L⁻¹ modifier (PP and FePP) in DMF
150 was drop-coated onto unmodified buckypaper surfaces with Ø
151 = 10 mm (each electrode contains 5.39 mg of MWCNTs) and
152 the resulting electrode left to dry overnight at room
153 temperature. Electrical contact was obtained via a metal wire
154 with carbon paste. The back and sides of the electrode were
155 sealed with silicone paste. 156

Preparation of Redox-Embedded MWCNT Bucky-
paper Electrodes by One-Pot Method. A 1 mg mL⁻¹
158 MWCNT suspension was first prepared by the addition of 150
159 mg of nonfunctionalized MWCNTs into 150 mL of DMF. The
160 dispersion was then sonicated for 30 min prior to addition of
161 the modifier (PLQ, NQ, PP, and FePP). The modifier,
162 dissolved in a minimum volume of DMF, was slowly added
163 into the MWCNT suspension to give a final 0.6 mmol L⁻¹ or 2
164 mmol L⁻¹ modifier concentration. Prior to filtration, the
165 resulting suspension was sonicated for a further 30 min. After
166 rigorous shaking for 1 min, 66 mL of the suspension was
167 filtered, washed, and dried (as above for the unmodified
168 buckypaper) and the resulting buckypaper cut into electrodes
169 with Ø = 10 mm. Electrical contact was obtained via a metal
170 wire with carbon paste. The back and sides of the electrode
171 were sealed with silicone paste. 172

Preparation of Buckypaper Bioelectrodes. First, 5 mg
173 mL⁻¹ stock solutions of BOD and FADGDH were prepared in
174 0.1 mol L⁻¹ phosphate buffer at pH 7.0 and McIlvaine buffer at
175 pH 7.0 (0.2 mol L⁻¹ Na₂HPO₄, 0.1 mol L⁻¹ citric acid),
176 respectively. A total of 150 μL of 5 mg mL⁻¹ enzyme solution
177 (0.75 mg enzyme) was then added to the surface of a
178 buckypaper with Ø = 10 mm, and the enzyme solution was
179 allowed to fully absorb at 4 °C overnight. The electrode was
180 subsequently rinsed with the corresponding buffer before use. 181

Electrochemistry. Electrochemical measurements were
182 performed at room temperature using an Eco Chemie Autolab
183 PGSTAT 100 potentiostat running GPES 4.9 software or a
184 Biologic VMP3Multi Potentiostat with EC-lab software. For
185 half-cell testing, a conventional three-electrode cell setup was
186 used comprising a buckypaper working electrode (Ø = 10 mm),
187 a saturated calomel reference electrode (SCE with sat. KCl),
188 and a Pt wire counter-electrode. The complete fuel cell setup
189 comprised a one-pot protoporphyrin buckypaper with BOD
190 biocathode (BP_{PP}-BOD) and a one-pot phenanthroline
191 quinone buckypaper with FADGDH (BP_{PLQ}-FADGDH)
192 bioanode immersed in 20 mL of McIlvaine buffer at pH 7.0
193 with an interelectrode distance of 3 mm. Gas flows were set
194 qualitatively and moderately to obtain reproducible conditions. 195

196 Average catalytic current densities were obtained by subtracting
 197 the background current: the signal obtained without oxygen, for
 198 the cathode, and without glucose, for the anode. Fuel cell
 199 experiments were performed by recording a linear sweep
 200 polarization from the open circuit voltage (OCV) to 0.02 V
 201 with the anode connected to the counter and reference leads,
 202 and the cathode connected to the working lead. Power densities
 203 were obtained by dividing the power delivery by the surface
 204 area or volume of one electrode.

205 **Scanning Electron Microscopy.** Buckypaper electrodes
 206 with $\varnothing = 3$ mm were imaged using a FEI/Quanta FEG 250
 207 scanning electron microscope (Hillsboro, OR, USA) operating
 208 at an accelerating voltage of 5 kV without metal coating.

209 **Static Water Contact Angles.** Water contact angles were
 210 obtained at room temperature by delivering a 2 μ L droplet of
 211 distilled water onto the sample surface on a horizontal stage
 212 using a Dataphysics OCA 35 system. Multiple droplet
 213 measurements (8 or 9) were recorded per sample type.

214 ■ RESULTS AND DISCUSSION

215 **Characterization of Unmodified MWCNT and Redox-**
 216 **Embedded MWCNT Buckypaper Electrodes.** Pristine
 217 freestanding buckypaper prepared from filtration of CNT
 218 dispersions without additives tends to be fragile and difficult
 219 to manipulate. Our initial experiments established that the ability
 220 to handle pristine unmodified BP was improved when the
 221 amount of MWCNTs in the final product was increased by at
 222 least a factor of 2.³⁰ Redox-embedded BP was subsequently
 223 prepared in several steps (see [Experimental Section](#)) either by
 224 the addition of redox molecules to the MWCNTs dispersion
 225 before filtration (one-pot method) or after filtration by drop-
 226 coating onto the unmodified BP (drop-coat method). The BP
 227 functionalization is based on π - π stacking interactions between
 228 aromatic groups and CNT sidewalls. For all buckypapers, flat
 229 and reproducible disks were obtained after filtration ([Figure](#)
 230 [1A](#)), drying, and cutting ([Figure 1B](#) and [C](#), respectively). BP
 231 thicknesses ranged between 230 and 320 μ m (see [Table S1](#)).
 232 The variability in thickness results from differences in vacuum
 233 pressure and the MWCNTs dispersion.

234 Scanning electron microscopy was performed to evaluate the
 235 morphology of unmodified BP (BP, [Figure 1D](#)) and BP
 236 prepared from the one-pot method with redox molecules:
 237 protoporphyrin IX (BP_{PP}, [Figure 1E](#)), ferriprotoporphyrin IX
 238 (BP_{FePP}, [Figure 1F](#)), and 1,10-phenanthroline-5,6-dione
 239 (BP_{PLQ}, [Figure 1G](#)). The SEM images reveal that the BPs
 240 comprise a random and entangled network of MWCNTs with
 241 nanoscale porosity. The images show subtle evidence that
 242 functionalized BPs have a flatter and more compact topography
 243 compared to unmodified BP, suggestive of more intimate
 244 interactions between nanotubes in the presence of redox
 245 molecules via π - π stacking.

246 Cyclic voltammograms (CVs) of the $\text{Fe}(\text{CN})_6^{3-/4-}$ redox probe
 247 recorded at unmodified and BP_{PP} paper electrodes reveal a
 248 significant increase in peak current with a decrease in peak-to-
 249 peak separation (ΔE_p) following modification with proto-
 250 porphyrin molecules (see [Figure S1](#)). The dramatic enhance-
 251 ment with chemical functionalization is partially attributed to a
 252 physical improvement in the electronic connectivity between
 253 carbon nanotubes. The increase in peak current observed is also
 254 partially attributed to improved diffusion of $\text{Fe}(\text{CN})_6^{3-/4-}$ in
 255 the 3D-structured electrode, facilitated by the increased surface
 256 hydrophilicity ([Figure S2](#)).

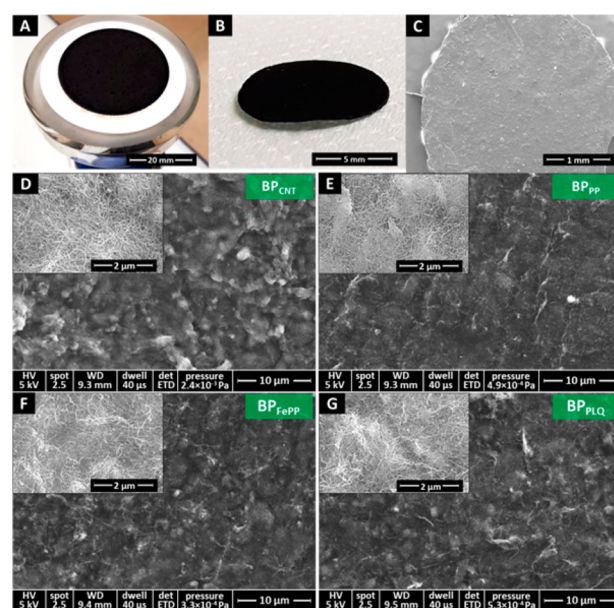


Figure 1. (A, B) Photographs of freshly prepared BP_{PP} buckypaper (A) after filtration and (B) after filtration, drying, and cutting into the electrode. (C–G) SEM micrographs of (C, E) BP_{PP}, (D) BP, (F) BP_{FePP}, and (G) BP_{PLQ} buckypaper electrodes recorded at (C) 60 \times , (D–G) 5000 \times and 40 000 \times (inset) magnification. All modified electrodes were prepared by the one-pot method.

To investigate the presence and accessibility of porphyrin
 and PLQ molecules in BP prepared via the one-pot and drop-
 coat methods, cyclic voltammetry was performed on one-sided
 BP samples with a geometric surface area of 0.785 cm². CVs
 were first recorded at functionalized electrodes prepared by the
 one-pot method in argon-saturated 0.1 mol L⁻¹ phosphate
 buffer at pH 7.0. [Figure 2](#) shows CVs recorded at BP_{FePP} and
 BP_{PLQ} prepared via the one-pot method. The CVs reveal the
 presence of well-defined chemically reversible processes. At
 BP_{FePP}, the one-electron Fe^{III}/Fe^{II} redox couple is observed at
 $E_{1/2} = -0.38$ V vs SCE (10 mV s⁻¹), consistent with reported

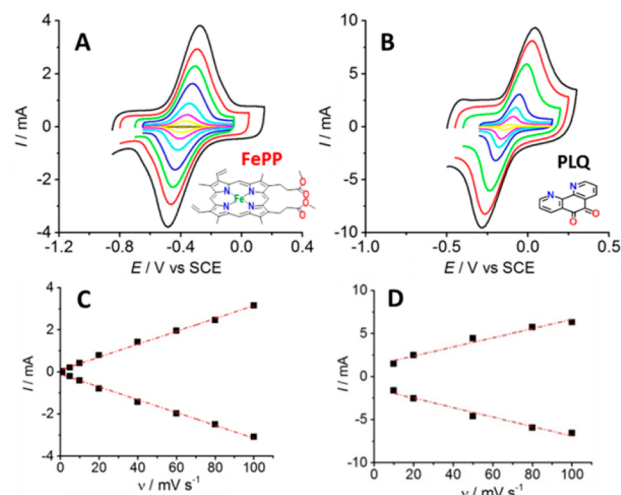


Figure 2. (A,B) CVs recorded at (A) BP_{FePP} and (B) BP_{PLQ} buckypaper electrodes (one-pot method) in Ar saturated 0.1 mol L⁻¹ phosphate buffer at pH 7 at different scan rates. (C, D) Corresponding plots of anodic and cathodic peak current versus scan rate.

Table 1. Electrochemical Parameters for BP_{FePP} and BP_{PLQ} Electrodes Prepared by One-Pot and Drop-Coating Functionalization Methods

buckypaper electrode (number ^a)	fabrication method	modifier concentration (mmol L ⁻¹)	surface concentration ^b (10 ⁻⁷ mol cm ⁻²)	ΔE _p (mV)	E _{1/2} (V)
BP _{FePP} (n = 3)	one-pot	0.6	1.38 ± 0.58	65	-0.37
BP _{FePP} (n = 3)	drop-coat	0.6	0.48 ± 0.25	55	-0.35
BP _{FePP} (n = 7)	drop-coat	10	6.43 ± 3.58	215	-0.36
BP _{PLQ} (n = 3)	one-pot	2	1.21 ± 0.30	118	-0.13

^aNumber of independent buckypaper electrode samples analyzed. ^bSurface concentrations obtained from the anodic peak of CVs recorded at 10 mVs⁻¹ in Ar.

values of E_{1/2} = -0.34 V and -0.39 V vs SCE for FePP modified MWCNTs on GC.^{33,34} At BP_{PLQ} the two-electron two-proton o-quinone/o-hydroquinone system is observed at E_{1/2} = -0.13 V vs SCE (10 mV s⁻¹) as previously observed for PLQ adsorbed on MWCNTs on GC electrodes.³⁵

Well-defined voltammograms and a linear dependence (r² > 0.95) of peak current on scan rate for anodic and cathodic peaks are observed at the BP_{FePP} and BP_{PLQ} electrodes (Figure 2C and D), confirming that the redox molecules are accessible and surface bound. The stability of the immobilized molecules was tested by subjecting the electrodes to repeat potential cycling at 20 mV s⁻¹ (Figure S3). No noticeable loss in electroactivity was observed after 20 cycles, confirming the high stability of the immobilized redox groups and the bulk nanotube structure despite the noncovalent modification approach.

Modified BP_{FePP} electrodes prepared by the drop-coat method were also examined by voltammetry and gave the expected electroactivity as observed for the one-pot method. BP_{FePP} electrodes were prepared by drop-coating 150 μL of 0.6 mmol L⁻¹ or 10 mmol L⁻¹ FePP DMF solutions onto pristine unmodified BPs (Ø = 10 mm). The electrochemical parameters obtained from CVs recorded in phosphate buffer at pH 7.0 and 10 mV s⁻¹ are listed in Table 1.

Examination of the data in Table 1 reveals that one-pot BP_{FePP} exhibits a higher surface concentration than drop-coat BP_{FePP} (1.38 ± 0.58 versus 0.48 ± 0.25 × 10⁻⁷ mol cm⁻²) when the same initial modifier concentration is used, consistent with effective bulk functionalization via the one-pot method. Increasing the modifier concentration from 0.6 mmol L⁻¹ to 10 mmol L⁻¹ resulted in a very high surface concentration of 6.43 ± 3.58 × 10⁻⁷ mol cm⁻², highlighting the possibility to tailor redox molecule loading in the paper electrodes. It is expected that such high surface concentrations would be possible via the one-pot method with a 10 mmol L⁻¹ modifier concentration. However, this was not explored due to the high volumes and quantity of modifier required for one-pot buckypaper fabrication. The surface concentrations for FePP prepared here are significantly higher than previously reported values of 6.8 × 10⁻¹⁰ mol cm⁻² and 1.1 × 10⁻⁹ mol cm⁻² for FePP modified MWCNTs on GC.^{33,34} The high loadings observed here are consistent with an effective high surface area 3D-structured matrix.

Table 1 also reveals that BP_{FePP} prepared via one-pot and drop-coat methods with 0.6 mmol L⁻¹ modifier solution give similar peak-to-peak separation values of ≤65 mV and therefore similar apparent electron transfer kinetics. Significantly larger ΔE_p values and therefore sluggish electron transfer kinetics were observed for highly functionalized BP_{FePP} electrodes prepared with 10 mmol L⁻¹ of the modifier. This is consistent with an extensive network of redox molecules being deeply

embedded in the CNT structure, which would increase electron tunneling distances and film resistivity.

On the basis of the BP_{FePP} optimization experiments, we prepared PLQ buckypaper via the one-pot method using a modestly high concentration of 2 mmol L⁻¹. No further optimization was performed. The surface concentration obtained for one-pot BP_{PLQ} was 1.21 ± 0.30 × 10⁻⁷ mol cm⁻², which reveals the possibility to obtain high redox molecule loadings with a near 1 × 10⁻⁷ mol cm⁻² concentration. The ΔE_p value of 118 mV observed for BP_{PLQ} is consistent with a slow rate of electron transfer, increased BP resistivity, and a large degree of potential inversion for the two-electron two-proton quinone process.³⁶

Bioelectrocatalytic O₂ Reduction at BP_{pp} Electrodes with Immobilized BOD Enzyme from *Myrothecium verrucaria*. For biocathode construction, the multicopper oxidase (MCO) enzyme BOD from *Myrothecium verrucaria* (Mv) was employed as the catalyst for the four-electron reduction of O₂ to H₂O. BOD is a promising enzyme for biofuel cells due to its high bioelectrocatalytic activity under mild conditions and formal potential close to that of the O₂/H₂O couple (0.816 V vs RHE at pH 0). Bilirubin, as a natural substrate for BOD, and its analogues, have been attached to MWCNT electrodes to facilitate DET with MvBOD for O₂ reduction.^{34,37} The interaction is supported by favorable immobilization and orientation. However, a commonly accepted problem with BOD is that significant catalytic activity loss is observed in the presence of H₂O₂, a common byproduct of oxidase enzymes found in glucose/O₂ biofuel cells. The use of O₂-insensitive FADGDH in biofuel cell design can circumvent this issue.

In this study, the porphyrin-BOD system was exploited for the development of buckypaper cathodes. One-pot BP_{pp} electrodes were first prepared then incubated with BOD, washed with phosphate buffer at pH 7.0, then tested for enzyme presence and activity. Figure 3A and B show CVs recorded in argon and oxygen at one-pot BP_{pp}-BOD and BP-BOD, respectively. Under oxygen, both types of electrode exhibited similar onset potential of E_{onset} = 0.54 ± 0.01 V vs SCE and 0.52 ± 0.01 V vs SCE, respectively. The onset potentials are close to that of the predicted T1 copper site of MvBOD responsible for substrate oxidation and successive electron transfers (E_{1/2(T1)} = 0.48 V vs SCE at pH 7.0).³⁴ The onset potentials are close to the ideal thermodynamic reduction potential for O₂ of 0.572 V vs SCE at pH 7.0 (assuming a potential difference of 244 mV between RHE and SCE reference electrodes). The onset potential values are therefore very attractive for biofuel cell applications and consistent with efficient single-proton single-electron DET between the BP and the enzyme.

The catalytic wave observed in oxygen at BP_{pp} confirms DET accompanied by the electrocatalytic reduction of oxygen via

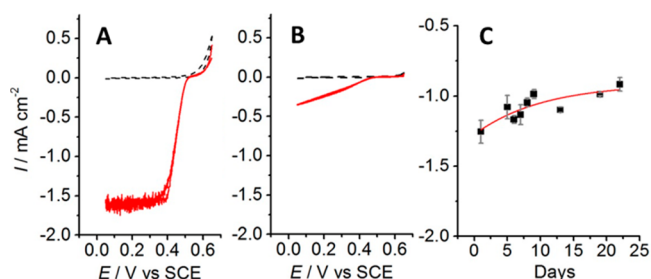


Figure 3. (A,B) CVs of bioelectrocatalytic O₂ reduction recorded at (A) BP_{PP} (one-pot method) and (B) BP buckypaper electrodes after BOD enzyme immobilization in (–) Ar saturated and (–) O₂ saturated 0.1 mol L^{−1} phosphate buffer at pH 7.0 at scan rate = 0.2 mV s^{−1}. (C) Evolution of maximum catalytic current density as a function of time for BP_{PP}-BOD. Chronoamperograms recorded at E_{app} = 0.2 V vs SCE and current densities obtained after 30 min. Error bars correspond to one standard deviation from two electrodes.

371 BOD. On the basis of repeat measurements, an average
372 maximum current density of $0.34 \pm 0.15 \text{ mA cm}^{-2}$ is observed
373 at BP compared to $1.33 \pm 0.17 \text{ mA cm}^{-2}$ for BP_{PP} (one-pot
374 method), confirming substantially enhanced performance for
375 the protoporphyrin buckypaper. At BP, an ill-defined “residual
376 slope” current is observed in oxygen, attributed to unfavorable
377 orientation of adsorbed enzymes. In contrast, at the BP_{PP}
378 electrode, well-defined steady-state voltammograms are ob-
379 served consistent with fast mass transport, enzyme catalysis,
380 and heterogeneous electron transfer at the buckypaper
381 electrode.³⁷ It is noted that a scan rate of 0.2 mV s^{−1} was
382 employed due to the superior steady-state signals with low
383 capacitance (see Figure S4 for catalytic currents recorded at
384 different scan rates). A summary of the catalytic parameters
385 obtained at different bioelectrodes is shown in Table 2.

Table 2. Catalytic Parameters for BP_{PP}-BOD Cathode and BP_{PLQ}-FADGDH Anode Prepared by One-Pot and Drop-Coating Functionalization Methods

buckypaper electrode (number ^a)	fabrication method (modifier concentration)	onset potential (V) ^b	maximum catalytic current (mA cm ^{−2}) ^{b,c}
BP _{PP} -BOD (n = 5)	one-pot (0.6 mmol L ^{−1})	0.54 ± 0.01	1.33 ± 0.17
BP _{PP} -BOD (n = 3)	drop-coat (0.6 mmol L ^{−1})	0.54 ± 0.01	1.10 ± 0.14
BP _{PP} -BOD (n = 3)	drop-coat (10 mmol L ^{−1})	0.54 ± 0.01	1.26 ± 0.11
BP-BOD (n = 3)	unmodified	0.52 ± 0.01	0.34 ± 0.15
BP _{PLQ} -FADGDH (n = 5)	one-pot (2 mmol L ^{−1})	-0.23 ± 0.01	5.38 ± 0.54
BP-FADGDH (n = 2)	unmodified	-0.01 ± 0.00	0.002 ± 0.001

^aNumber of independent buckypaper electrode samples analyzed.
^bParameters obtained from the forward sweep of CVs recorded at 0.2 mV s^{−1}. ^cCurrent obtained at 0.2 and 0.15 V at BOD and FADGDH electrodes, respectively.

386 The long-term stability of BP_{PP}-BOD was also assessed by
387 periodically recording chronoamperograms at E_{app} = 0.2 V vs
388 SCE for 30 min over 24 days of storage in phosphate buffer at
389 pH 7.0 (Figure S5). The corresponding plot in Figure 3C of the
390 maximum catalytic current obtained on different days reveals
391 remarkable stability for BP_{PP}-BOD, with the current density

decreasing by 10% over the first 7 days and 27% over 24 days.
392 Stability experiments performed in a similar manner at other
393 MWCNT-MCO enzyme cathodes report 40–45% current loss
394 after 1 week and 45–60% after 20–24 days.^{38,39} To clarify, such
395 stability experiments evaluate both operational stability (for 30
396 min per day) and storage stability. The enhanced stability
397 observed here compared to that with CNT-modified GC
398 electrodes is consistent with improved physical enzyme
399 entrapment into the nanopore-containing CNT matrix via
400 fixation and/or dynamic reorganization effects.⁴⁰

A brief assessment of the bioelectrocatalytic performance of
402 BP_{PP}-BOD was also performed to demonstrate enzyme
403 inhibition at the biocathode. CVs recorded in the presence
404 and absence of 40 mmol L^{−1} H₂O₂ in phosphate buffer at pH
405 7.0 in oxygen are shown in Figure S6 and clearly reveal the loss
406 of oxygen reduction current due to inhibition of immobilized
407 bilirubin oxidase by H₂O₂. The catalytic current was suppressed
408 in the presence of H₂O₂ and remained suppressed after transfer
409 to a fresh phosphate buffer solution, confirming that the
410 enzyme’s activity was inhibited and not restored. The absence
411 of oxygen reduction in these experiments validates the
412 importance of the active “wired” enzyme as the biocatalyst.
413 Chronoamperometry performed at BP_{PP}-BOD in phosphate
414 buffer at pH 7.0 in oxygen (Figure S6) revealed the rapid
415 nature of enzyme inhibition by H₂O₂ and the good stability of
416 the biocathode in the presence of a physiologically relevant
417 concentration of NaCl (100 mM).

The bioelectrocatalytic performance of BP_{PP} for oxygen
419 reduction was also performed at electrodes prepared by the
420 drop-coat method. No significant difference in E_{onset} was
421 observed between drop-coat and one-pot BP_{PP} electrodes.
422 Likewise, equivalent sigmoidal steady-state current responses
423 (with different current magnitudes) were observed for all BP_{PP}
424 electrodes. For drop-coat BP_{PP}, the maximum average catalytic
425 current only slightly increased from 1.10 ± 0.14 to 1.26 ± 0.11
426 mA cm^{−2} with an increase in protoporphyrin modifier from 0.6
427 mmol L^{−1} to 10 mmol L^{−1}.

The best performing biocathode identified here was the
429 BP_{PP}-BOD prepared using the one-pot method with I_{max} = 1.33
430 $\pm 0.17 \text{ mA cm}^{-2}$. The high performance of this biocathode is
431 clear given that typical values obtained by our group and others
432 for CNT paper-based MCO cathodes are 0.17 to 1.1 mA cm^{−2}
433 in oxygen-saturated solution.^{27,29,30,41,42}

Bioelectrocatalytic Glucose Oxidation at BP_{PLQ} Electrodes with Immobilized FADGDH from *Aspergillus sp.*
435 For bioanode development, the one-pot method was exploited
436 for preparation of a new type of redox-embedded buckypaper
437 with immobilized FADGDH. To prepare the anode, a
438 MWCNT dispersion containing 2 mmol L^{−1} of 1,10-
439 phenanthroline-5,6-dione (PLQ) was used. The bioanode was
440 obtained by drop-casting 150 μL of 5 mg mL^{−1} enzyme
441 solution onto the BP_{PLQ} and leaving the solution overnight
442 until the droplet had fully adsorbed. The PLQ molecule has
443 previously been reported as a mediator for the cofactors
444 NADH/NADPH coupled with NAD/NADP-dependent en-
445 zymes.^{35,43} To the best of our knowledge, the phenanthroline
446 quinone as a free ligand has not been demonstrated as a
447 mediator for FAD-dependent enzymes such as FADGDH. In
448 addition to the low redox potentials, a major advantage of
449 phenanthroline quinone mediators is their nonreactivity toward
450 active-site enzyme amine and thiol groups.⁴³ In this work, we
451 have investigated the use of PLQ₂ in the form of a redox-
452 embedded functionalized buckypaper, to electrically connect
453

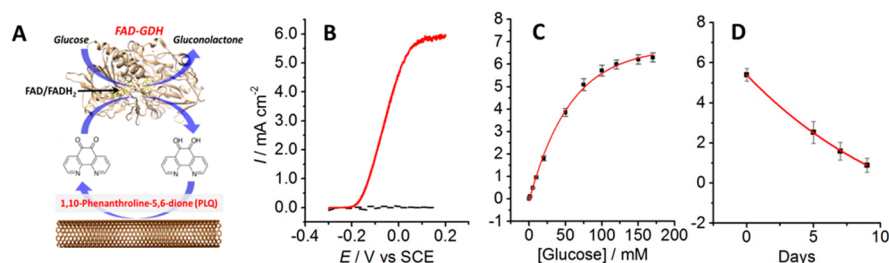


Figure 4. (A) Scheme illustrating bioelectrocatalytic oxidation of glucose on BP_{PLQ} buckypaper via MET with the active site of FADGDH. (B) CVs recorded at a BP_{PLQ} buckypaper electrode after FADGDH immobilization in (--) 0 mmol L⁻¹ and (—) 170 mmol L⁻¹ glucose in Ar saturated McIlvaine buffer at pH 7.0 at scan rate = 0.2 mV s⁻¹. (C) Plot of average current density obtained for different glucose concentrations recorded at three BP_{PLQ}-FADGDH electrodes. (D) Evolution of maximum catalytic current density as a function of time for BP_{PLQ}-FADGDH with 170 mmol L⁻¹ glucose. (C, D) Chronoamperograms recorded at $E_{\text{app}} = 0.15$ V vs SCE and current densities obtained after 30 min. Error bars correspond to one standard deviation from at least two electrodes.

455 the active site of FADGDH to the electrode for bioelec-
 456 trocatalytic oxidation of glucose (see Figure 4A). In this
 457 mechanism, the FADGDH oxidizes the β -D-glucose to D-
 458 glucono-1,5-lactone using the FAD cofactor, which itself is
 459 reduced to FADH₂. The PLQ mediator then acts as a
 460 secondary electron acceptor to oxidize the reduced cofactor,
 461 FADH₂. The mediator is finally reoxidized by the electrode
 462 which is set at an appropriate oxidizing potential.

463 Figure 4B and Figure S7 show CVs recorded in 0 (--) and
 464 170 mmol L⁻¹ (—) glucose in McIlvaine buffer at pH 7.0 at
 465 one-pot BP_{PLQ}-FADGDH and BP-FADGDH electrodes,
 466 respectively. In the presence of 170 mmol L⁻¹ glucose, an
 467 onset potential of $E_{\text{onset}} = -0.23 \pm 0.01$ V vs SCE is observed at
 468 BP_{PLQ}-FADGDH, which is attractively low for a glucose-
 469 oxidizing bioanode and similar to that obtained using 1,4
 470 naphthoquinone hydrogel mediators with FADGDH ($E_{\text{onset}} =$
 471 -0.18 to -0.25 V vs SCE at near neutral pH).^{22,23}
 472 Interestingly, the onset potential of -0.23 V is much more
 473 negative than the ≈ -0.05 V previously reported using a Ru-
 474 PLQ polymer with FADGDH,²⁰ highlighting an advantage of
 475 using the free PLQ mediator in this form. The onset potential is
 476 around 180 mV positive of the estimated redox potential of
 477 -0.41 V vs SCE for the enzyme-bound relay, FAD/FADH₂,
 478 consistent with thermodynamically attractive electron wiring.²²
 479 The onset potential at BP_{PLQ} for glucose oxidation is also about
 480 200 mV more negative than ferrocene and osmium mediator-
 481 modified electrodes with $E_{\text{onset}} \approx -0.05$ to 0.15 V vs
 482 SCE,^{17,19,21} and thus PLQ is an attractive mediator for biofuel
 483 cell applications.

484 The voltammograms recorded at BP_{PLQ} under argon in the
 485 absence and presence of 170 mmol L⁻¹ glucose clearly
 486 demonstrate a drastic increase in current signal with glucose
 487 addition. Well-defined sigmoidal waves are observed at 0.2 mV
 488 s⁻¹ consistent with electrocatalytic oxidation of glucose. A
 489 maximum current density of 5.38 ± 0.54 mA cm⁻² is observed
 490 at 0.15 V at BP_{PLQ} without stirring. In contrast, voltammograms
 491 recorded at BP under the same conditions reveal a negligible
 492 maximum current density of 0.002 ± 0.001 mA cm⁻². The
 493 substantial enhancement in catalytic current provides compel-
 494 ling evidence for mediated electron transfer reaction via PLQ.
 495 The high catalytic currents obtained were subsequently
 496 validated by comparison with a CNT paper prepared using a
 497 known mediator for FADGDH. A 1,4 naphthoquinone
 498 buckypaper, BP_{NQ}-FADGDH, was prepared and tested in the
 499 same manner as for BP_{PLQ}-FADGDH. Voltammetry revealed a
 500 significantly smaller maximum current density of 2.20 mA cm⁻²
 501 (Figure S8). Despite being less powerful than the BP_{PLQ}

502 electrode, the BP_{NQ} electrode still exceeds recent high
 503 performance NQ-anodes.^{22,23}

504 The catalytic current obtained of 5.38 ± 0.54 mA cm⁻² at
 505 0.15 V vs SCE for BP_{PLQ} in unstirred solution exceeds the
 506 performance of that observed at most bioanodes to date
 507 without the use of hydrodynamic conditions. We believe that
 508 the BP_{PLQ} anode exhibits the highest catalytic density for
 509 glucose oxidation of any paper-based bioanode. At phenothia-
 510 zine-modified commercial buckypaper with immobilized NAD-
 511 dependent GDH and NAD cofactor, current densities up to 2.6
 512 mA cm⁻² at 25 °C have been reported.²⁵ With the addition of 1
 513 mmol L⁻¹ NAD⁺ in solution, the catalytic current increased to
 514 4.5 mA cm⁻² at a high potential of 0.35 V. In addition to the
 515 high potential required, the use of NAD in solution is less
 516 convenient than if the cofactor is surface-bound or enzyme-
 517 bound. High performing bioanode architectures typically
 518 produce no more than 2 mA cm⁻² with the exception
 519 of a hierarchical porous carbon bioelectrode which exhibited
 520 enormous densities up to 100 mA cm⁻² with rapid
 521 convection.¹⁸ With CNT-modified Toray papers with immo-
 522 bilized glucose oxidase and dehydrogenases, current densities in
 523 the range 1–3.3 mA cm⁻² have been reported.^{23,46–48}

524 Evaluation of the steady-state current at a fixed potential of
 525 0.15 V as a function of glucose concentration reveals a linear
 526 increase in the range 1 mmol L⁻¹ to 50 mmol L⁻¹ (see
 527 calibration plot in Figure S9). As a side note, the linearity of r^2
 528 = 0.996 and the ability to detect beyond the upper limit of 30
 529 mmol L⁻¹ means that the BP_{PLQ}-FADGDH meets basic
 530 requirements for a commercial glucose sensor.

531 Figure 4C shows that the steady-state currents increased with
 532 increasing concentration to a plateau at 170 mmol L⁻¹ glucose;
 533 hence 170 mmol L⁻¹ was adopted in experiments as the
 534 concentration to maximize catalytic current output, limited by
 535 the enzymatic reaction and catalyst surface coverage. Limiting
 536 current values were reached within 30 s (Figure S10),
 537 consistent with fast mass transport of glucose at the electrode.
 538 Estimated values for the apparent Michaelis–Menten and
 539 velocity constants of $K_m = 40.4$ mmol L⁻¹ and $V_{\text{max}} = 6.1$ mA
 540 cm⁻², respectively, are obtained. The estimated K_m is similar to
 541 that observed for fungal FADGDHs ($K_m = 35$ mmol L⁻¹),⁴⁹
 542 and hence the BP_{PLQ} electrode maximizes electrocatalysis
 543 without significantly affecting the enzymes' binding constant for
 544 glucose.

545 The stability of the BP_{PLQ}-FADGDH bioanode was assessed
 546 over 10 days by periodically recording chronoamperograms at
 547 $E_{\text{app}} = 0.15$ V vs SCE for 30 min in McIlvaine buffer at pH 7.0
 548 (Figure S11). The plot in Figure 4D of the maximum catalytic
 549

549 current obtained on different days reveals that the bioanode is
550 significantly less stable than the biocathode. After 2 days, 75%
551 of the original current remains. After 5 days, only 48% of the
552 initial current remains. Similar storage stability for an
553 FADGDH electrode has previously been observed using an
554 Os polymer mediator with 80% of the initial current observed
555 after 2 days followed by a rapid breakdown to 56% after 6
556 days.¹³ This finding suggests that PLQ may be no less toxic or
557 inhibitory toward FADGDH than osmium polymers. Despite
558 the poor stability, high maximum current densities of ≈ 1 mA
559 cm^{-2} are nevertheless possible after 10 days, confirming that
560 the BP_{PLQ} is operational for several days.

561 Assessment of the bioelectrocatalytic performance of BP_{PLQ}-
562 FADGDH was also performed to explore enzyme inhibition at
563 the bioanode. CVs recorded before and after the addition of 10
564 mmol L^{-1} of CuCl_2 in McIlvaine buffer at pH 7.0 are shown in
565 Figure S12 and clearly reveal the loss of glucose oxidation
566 current due to inhibition of immobilized FADGDH, attributed
567 to binding of Cu^{2+} to the FADH₂ cofactor as previously
568 observed for glucose oxidase.⁵⁰ The possibility to reverse the
569 enzyme inhibition by addition of a strong metal chelator to
570 reverse binding of the metal ions to FAD was also tested. The
571 voltammogram obtained after addition of an excess of
572 ethylenediaminetetracetic acid (EDTA, 11 mmol L^{-1}) and
573 mild stirring shows an increase in the catalytic oxidation current
574 on the reverse sweep, attributed to partial reactivation of the
575 biocatalyst.

576 **Single Compartment Biofuel Cell with a BP_{PP}-BOD**
577 **Cathode and BP_{PLQ}-FADGDH Anode Prepared via One-**
578 **Pot Fabrication.** Power generation from membraneless
579 glucose/oxygen biofuel cells using redox-embedded bucky-
580 papers was subsequently investigated. A single-compartment
581 glucose/ O_2 paper-based biofuel cell was constructed using a
582 BP_{PP}-BOD cathode and a BP_{PLQ}-FADGDH anode prepared via
583 one-pot methods (Figure 5A). Linear polarization curves were

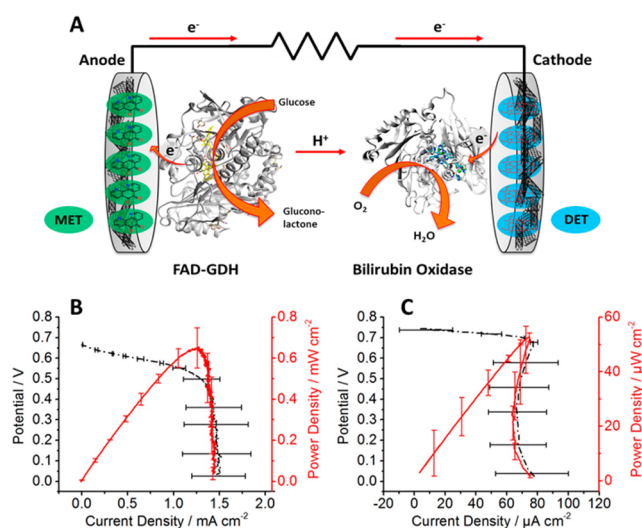
584 recorded at 0.2 mV s^{-1} in McIlvaine buffer at pH 7.0 to evaluate
585 the performance under oxygen-saturated (≈ 1.1 mmol L^{-1}) and
586 quiescent oxygen conditions (≈ 0.23 mmol L^{-1}) with 170
587 mmol L^{-1} glucose.⁵¹ Large OCVs of 0.74 ± 0.01 V and $0.67 \pm$
588 0.01 V were obtained under quiescent and oxygen-saturated
589 conditions, respectively. The OCVs match closely the estimated
590 maximum voltage of 0.77 V from the half-cell polarization
591 experiments. The difference in OCV between the quiescent and
592 oxygen-saturated conditions is attributed to a small amount of
593 degradation between fuel cell testing experiments.

594 Average polarization and power curves (Figure 5B and C)
595 reveal a maximum power density of 0.65 ± 0.10 mW cm^{-2} or
596 24.07 mW cm^{-3} at 0.5 V for the biofuel cell under oxygen-
597 saturated conditions without stirring. Under quiescent oxygen
598 with no stirring, a maximum power density of 0.053 mW cm^{-2}
599 or 1.97 mW cm^{-3} is observed. The power outputs for these
600 glucose/ O_2 biofuel cells are either very good or exceptional
601 depending on whether the power delivery is divided by the
602 surface area (cm^2) or volume (cm^3). It is noted that we used
603 equal sized anodes and cathodes in this work and that the
604 power densities were obtained by dividing the power delivery
605 by either the surface area or volume of one electrode. Given
606 that buckypaper is a three-dimensional electrode and size is a
607 crucial parameter for portable biofuel cell applications, the
608 power density in mW cm^{-3} is arguably more appropriate.
609 However, for this work we have chosen to remain with the
610 standard mW cm^{-2} convention for figures. Maximum power
611 outputs for a single EBFC in the literature are between 1.45 and
612 2.3 mW cm^{-2} at 0.3 to 0.55 V.^{22,23,52} One of these previously
613 reported biofuel cells, based on our estimates, gives up to 3.8
614 mW cm^{-3} (1.54 mW cm^{-2}), and thus the delivery of 24.07
615 mW cm^{-3} reported here is markedly high.

616 The difference in power density observed between the
617 saturated and quiescent oxygen conditions reveals that the
618 biofuel cell is strongly limited by oxygen availability at the
619 cathode. Even in the presence of oxygen-saturated conditions,
620 the biocathode is limiting.

621 Polarization and power curves were also recorded at freshly
622 prepared biofuel cells in the absence of glucose under oxygen-
623 saturated conditions as control experiments (Figure S13). In
624 the absence of the enzyme's substrate, the low power output
625 and a small OCV, namely 0.02 mW cm^{-2} and 0.53 ± 0.02 V,
626 clearly illustrate and confirm the unambiguous role of
627 FADGDH and the need for glucose for effective biofuel cell
628 performance.

629 In order to assess the operational stability of the biofuel cell,
630 potentiostatic and galvanostatic tests were performed for 30
631 min. This duration may, for example, be considered as an
632 adequate operational time for a single use self-powered
633 biosensor. The stability of the biofuel cell was first examined
634 by applying a mild fixed voltage of 0.2 V and monitoring the
635 current in oxygen-saturated solution. The power obtained from
636 the recorded current revealed a stable power output of $295 \pm$
637 25 $\mu\text{W cm}^{-2}$ after an initial 30 s induction period (Figure 6A).
638 Similar glucose/oxygen biofuel cell stability has been observed
639 using FADGDH, which, notably, is vastly superior to that
640 observed with the GOx enzyme.¹⁴ The initial induction period
641 is attributed to diffusional equilibration and high charging
642 currents. To further assess the stability, a current of 500 μA
643 was continuously drawn and the evolution of voltage monitored
644 (Figure 6B). Following the short initial induction period, a
645 stable voltage of 0.57 ± 0.01 V is obtained.



646 **Figure 5.** (A) Scheme illustrating the single compartment buckypaper
647 biofuel cell comprising an O_2 reducing BP_{PP}-BOD cathode and glucose
648 oxidizing BP_{PLQ}-FADGDH anode. (B, C) Biofuel cell polarization (---)
649 and power curves (—) recorded under (B) oxygen-saturated and (C)
650 quiescent oxygen conditions in McIlvaine buffer at pH 7.0 with 170
651 mmol L^{-1} glucose. Polarization voltammograms were recorded at 0.2
652 mV s^{-1} . Error bars correspond to one standard deviation from three
653 biofuel cells.

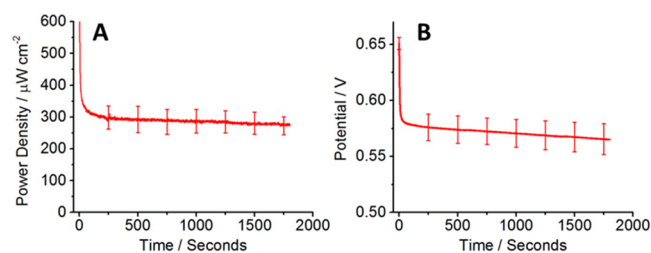


Figure 6. (A) Power generated from current discharge at 0.2 V and (B) voltage generated at $600 \mu\text{A cm}^{-2}$ ($500 \mu\text{A}$) for 30 min operation of the BP_{PP}-BOD/BP_{PLQ}-FADGDH biofuel cell in O₂ saturated McIlvaine buffer at pH 7.0 with 170 mmol L^{-1} glucose. Error bars correspond to one standard deviation from three biofuel cells.

646 ■ CONCLUSIONS

647 Electricity generation from glucose and oxygen using small and
 648 lightweight enzymatic biofuel cells opens up the attractive
 649 prospect of self-powered health and environmental sensor
 650 devices. Here, we report the fabrication of new freestanding
 651 redox-embedded (porphyrin, phenanthroline quinone, and
 652 naphthoquinone) carbon nanotube paper electrodes with
 653 physical durability, practical flexibility, and excellent electro-
 654 chemical properties. Elaboration of the electrodes for
 655 construction of bioelectrodes with high catalytic performance
 656 compared to literature values was subsequently demonstrated.
 657 Very high catalytic performance was observed by employing
 658 1,10-phenanthroline-5,6-dione as an electron transfer mediator
 659 with FADGDH at the anode. The biofuel cell delivers milliwatt
 660 per cubic centimeter power densities under either quiescent
 661 solution (dissolved oxygen) or saturated oxygen solution
 662 conditions, with 170 mmol L^{-1} glucose at neutral pH and
 663 room temperature. In addition, the half-cell and biofuel cell
 664 experiments show good operational stability, which could be
 665 appropriate for disposable self-powered sensors. We expect that
 666 the proposed fabrication methods, buckypapers, and use of
 667 PLQ for mediated electron transfer with FADGDH will
 668 advance the field of biofuel cells toward practical applications,
 669 especially considering the excellent prospects of the FADGDH
 670 enzyme and paper-based bioelectrodes. Future work is now
 671 required to address the limiting cathode power output under
 672 quiescent oxygen levels (for example, by enhancement of
 673 dioxygen mass transport) and the comparatively poor stability
 674 observed at the anode over several days (for example, via caging
 675 and shrinking effects).

676 ■ ASSOCIATED CONTENT

677 ■ Supporting Information

678 The Supporting Information is available free of charge on the
 679 ACS Publications website at DOI: 10.1021/acscatal.7b00738.

680 Electrode characterization and stability, Figures S1–S13
 681 (PDF)

682 ■ AUTHOR INFORMATION

683 Corresponding Authors

684 *E-mail: andrew.gross@univ-grenoble-alpes.fr.

685 *E-mail: serge.cosnier@univ-grenoble-alpes.fr.

686 ORCID

687 Andrew. J. Gross: 0000-0002-7356-7089

688 Xiaohong Chen: 0000-0002-6535-3873

689 Alan Le Goff: 0000-0002-6765-5859

Michael Holzinger: 0000-0003-3700-4673

690

Author Contributions

691

The manuscript was written through contributions of all
 692 authors. All authors have given approval to the final version of
 693 the manuscript.

694

Notes

695

The authors declare no competing financial interest.

696

■ ACKNOWLEDGMENTS

697

This work was supported by LabEx ARCANE (ANR-11-LABX-
 698 0003-01) and ANR-15-JTIC-0002-01. The region Auvergne-
 699 Rhône-Alpes is acknowledged for the Ph.D. funding of C.A.
 700 The authors would also like to thank the platform Chimie
 701 NanoBio ICMG FR 2607 (PCN-ICMG) and PFT “Surfaces
 702 Functionalization and Transduction” for providing facilities and
 703 PMIEL “Microscopy” for SEM imaging. We are very grateful to
 704 Christine Lancelon Pin for assistance with SEM imaging.
 705

■ REFERENCES

706

- (1) Cosnier, S.; Gross, A. J.; Le Goff, A.; Holzinger, M. *J. Power Sources* **2016**, *325*, 252–263. 707
- (2) Slaughter, G.; Kulkarni, T. J. *Biochips Tissue Chips* **2015**, *5* (111), 708 1–10. 709
- (3) Agnès, C.; Holzinger, M.; Le Goff, A.; Reuillard, B.; Elouarzaki, 710 K.; Tingry, S.; Cosnier, S. *Energy Environ. Sci.* **2014**, *7*, 1884–1888. 711
- (4) Zebda, A.; Cosnier, S.; Alcaraz, J.-P.; Holzinger, M.; Le Goff, A.; 712 Gondran, C.; Boucher, F.; Giroud, F.; Gorgy, K.; Lamraoui, H.; 713 Cinquin, P. *Sci. Rep.* **2013**, *3*, 370–375. 714
- (5) MacVittie, K.; Halámek, J.; Halámková, L.; Southcott, M.; 715 Jemison, W. D.; Lobel, R.; Katz, E. *Energy Environ. Sci.* **2013**, *6*, 81–86. 716
- (6) Halámková, L.; Halámek, J.; Bocharova, V.; Szczupak, A.; Alfonta, 717 L.; Katz, E. *J. Am. Chem. Soc.* **2012**, *134*, 5040–5043. 718
- (7) Cinquin, P.; Gondran, C.; Giroud, F.; Mazabrard, S.; Pellissier, 719 A.; Boucher, F.; Alcaraz, J.-P.; Gorgy, K.; Lenouvel, F.; Mathé, S.; 720 Porcu, P.; Cosnier, S. *PLoS One* **2010**, *5*, e10476. 721
- (8) Jia, W.; Valdés-Ramírez, G.; Bandonkar, A. J.; Windmiller, J. R.; 722 Wang, J. *Angew. Chem., Int. Ed.* **2013**, *52*, 7233–7236. 723
- (9) Ogawa, Y.; Kato, K.; Miyake, T.; Nagamine, K.; Ofuji, T.; 724 Yoshino, S.; Nishizawa, M. *Adv. Healthcare Mater.* **2015**, *4*, 506–510. 725
- (10) Pankratov, D.; González-Arribas, E.; Blum, Z.; Shleev, S. 726 *Electroanalysis* **2016**, *28*, 1250–1266. 727
- (11) Giroud, F.; Gross, A. J.; Faggion, D., Jr.; Holzinger, M.; Maduro 728 de Campos, C. E.; Acuña, J. J. S.; Domingos, J. B.; Cosnier, S. *J. Electrochem. Soc.* **2017**, *164*, H3052–H3057. 729
- (12) Arechederra, R. L.; Minteer, S. D. *Anal. Bioanal. Chem.* **2011**, 730 *400*, 1605–1611. 731
- (13) Zafar, M. N.; Beden, N.; Leech, D.; Sygmund, C.; Ludwig, R.; 732 Gorton, L. *Anal. Bioanal. Chem.* **2012**, *402*, 2069–2077. 733
- (14) Milton, R. D.; Giroud, F.; Thumser, A. E.; Minteer, S. D.; Slade, 734 R. C. T. *Phys. Chem. Chem. Phys.* **2013**, *15*, 19371–19379. 735
- (15) Shiota, M.; Yamazaki, T.; Yoshimatsu, K.; Kojima, K.; Tsugawa, 736 W.; Ferri, S.; Sode, K. *Bioelectrochemistry* **2016**, *112*, 178–183. 737
- (16) Saboe, P. O.; Conte, E.; Farrell, M.; Bazan, G. C.; Kumar, M. 738 *Energy Environ. Sci.* **2017**, *10*, 14–42. 739
- (17) Murata, K.; Akatsuka, W.; Sadakane, T.; Matsunaga, A.; 740 Tsujimura, S. *Electrochim. Acta* **2014**, *136*, 537–541. 741
- (18) Tsujimura, S.; Murata, K.; Akatsuka, W. *J. Am. Chem. Soc.* **2014**, 742 *136*, 14432–14437. 743
- (19) Pinyou, P.; Ruff, A.; Poeller, S.; Ma, S.; Ludwig, R.; Schuhmann, 744 W. *Chem. - Eur. J.* **2016**, *22*, 5319–5326. 745
- (20) Sakuta, R.; Takeda, K.; Ishida, T.; Igarashi, K.; Samejima, M.; 746 Nakamura, N.; Ohno, H. *Electrochem. Commun.* **2015**, *56*, 75–78. 747
- (21) Milton, R. D.; Lim, K.; Hickey, D. P.; Minteer, S. D. 748 *Bioelectrochemistry* **2015**, *106*, 56–63. 749
- (22) Hou, C.; Lang, Q.; Liu, A. *Electrochim. Acta* **2016**, *211*, 663– 750 670. 751

- 754 (23) Milton, R. D.; Hickey, D. P.; Abdellaoui, S.; Lim, K.; Wu, F.;
755 Tan, B.; Minter, S. D. *Chem. Sci.* **2015**, *6*, 4867–4875.
- 756 (24) Ravenna, Y.; Xia, L.; Gun, J.; Mikhaylov, A. A.; Medvedev, A. G.;
757 Lev, O.; Alfonta, L. *Anal. Chem.* **2015**, *87*, 9567–9571.
- 758 (25) Narváez Villarrubia, C. W.; Artyushkova, K.; Garcia, S. O.;
759 Atanassov, P. *J. Electrochem. Soc.* **2014**, *161*, H3020–H3028.
- 760 (26) Cosnier, S.; Holzinger, M.; Le Goff, A. *Front. Bioeng. Biotechnol.*
761 **2014**, *2*, 2296–4185.
- 762 (27) Bunte, C.; Hussein, L.; Urban, G. A. *J. Power Sources* **2014**, *247*,
763 579–586.
- 764 (28) Narvaez Villarrubia, C. W.; Soavi, F.; Santoro, C.; Arbizzani, C.;
765 Serov, A.; Rojas-Carbonell, S.; Gupta, G.; Atanassov, P. *Biosens.*
766 *Bioelectron.* **2016**, *86*, 459–465.
- 767 (29) Bourourou, M.; Elouarzaki, K.; Holzinger, M.; Agnès, C.; Le
768 Goff, A. L.; Reverdy-Bruas, N.; Chaussy, D.; Party, M.; Maaref, A.;
769 Cosnier, S. *Chem. Sci.* **2014**, *5*, 2885–2888.
- 770 (30) Gross, A. J.; Robin, M. P.; Nedellec, Y.; O'Reilly, R. K.; Shan,
771 D.; Cosnier, S. *Carbon* **2016**, *107*, 542–547.
- 772 (31) Elouarzaki, K.; Bourourou, M.; Holzinger, M.; Le Goff, A.;
773 Marks, R. S.; Cosnier, S. *Energy Environ. Sci.* **2015**, *8*, 2069–2074.
- 774 (32) Reuillard, B.; Warnan, J.; Leung, J. J.; Wakerley, D. W.; Reiser,
775 E. *Angew. Chem., Int. Ed.* **2016**, *55*, 3952–3957.
- 776 (33) Reuillard, B.; Gentil, S.; Carrière, M.; Le Goff, A. L.; Cosnier, S.
777 *Chem. Sci.* **2015**, *6*, 5139–5143.
- 778 (34) Lalaoui, N.; Le Goff, A.; Holzinger, M.; Cosnier, S. *Chem. - Eur.*
779 *J.* **2015**, *21* (47), 16868–16873.
- 780 (35) Faggion, D. F., Jr.; Haddad, R.; Giroud, F.; Holzinger, M.;
781 Maduro de Campos, C. E. M. de; Acuña, J. J. S.; Domingos, J. B.;
782 Cosnier, S. *Nanoscale* **2016**, *8*, 10433–10440.
- 783 (36) Kim, R. S.; Chung, T. D. *Bull. Korean Chem. Soc.* **2014**, *35*,
784 3143–3155.
- 785 (37) So, K.; Kitazumi, Y.; Shirai, O.; Kano, K. *J. Electroanal. Chem.*
786 **2016**, *783*, 316–323.
- 787 (38) Lalaoui, N.; Rousselot-Pailley, P.; Robert, V.; Mekmouche, Y.;
788 Villalonga, R.; Holzinger, M.; Cosnier, S.; Tron, T.; Le Goff, A. *ACS*
789 *Catal.* **2016**, *6*, 1894–1900.
- 790 (39) Bourourou, M.; Elouarzaki, K.; Lalaoui, N.; Agnès, C.; Le Goff,
791 A.; Holzinger, M.; Maaref, A.; Cosnier, S. *Chem. - Eur. J.* **2013**, *19*,
792 9371–9375.
- 793 (40) Gutierrez-Sanchez, C.; Ciaccafava, A.; Blanchard, P. Y.;
794 Monsalve, K.; Giudici-Ortoni, M. T.; Lecomte, S.; Lojou, E. *ACS*
795 *Catal.* **2016**, *6*, 5482–5492.
- 796 (41) Hussein, L.; Rubenwolf, S.; von Stetten, F.; Urban, G.; Zengerle,
797 R.; Krueger, M.; Kerzenmacher, S. *Biosens. Bioelectron.* **2011**, *26*,
798 4133–4138.
- 799 (42) Scherbahn, V.; Putze, M. T.; Dietzel, B.; Heinlein, T.; Schneider,
800 J. J.; Lisdat, F. *Biosens. Bioelectron.* **2014**, *61*, 631–638.
- 801 (43) Forrow, N. J.; Sanghera, G. S.; Walters, S. J.; Watkin, J. L.
802 *Biosens. Bioelectron.* **2005**, *20*, 1617–1625.
- 803 (44) de Souza, J. C. P.; Iost, R. M.; Crespilho, F. N. *Biosens.*
804 *Bioelectron.* **2016**, *77*, 860–865.
- 805 (45) Cadet, M.; Gounel, S.; Stines-Chaumeil, C.; Brilland, X.;
806 Rouhana, J.; Louerat, F.; Mano, N. *Biosens. Bioelectron.* **2016**, *83*, 60–
807 67.
- 808 (46) Ivnitski, D.; Branch, B.; Atanassov, P.; Apblett, C. *Electrochem.*
809 *Commun.* **2006**, *8*, 1204–1210.
- 810 (47) Reid, R. C.; Giroud, F.; Minter, S. D.; Gale, B. K. *J. Electrochem.*
811 *Soc.* **2013**, *160*, H612–H619.
- 812 (48) Hickey, D. P.; Reid, R. C.; Milton, R. D.; Minter, S. D. *Biosens.*
813 *Bioelectron.* **2016**, *77*, 26–31.
- 814 (49) Sakai, G.; Kojima, K.; Mori, K.; Oonishi, Y.; Sode, K. *Biotechnol.*
815 *Lett.* **2015**, *37*, 1091–1099.
- 816 (50) Meredith, M. T.; Minter, S. D. *Anal. Chem.* **2011**, *83*, 5436–
817 5441.
- 818 (51) Yomo, T.; Urabe, I.; Okada, H. *Anal. Biochem.* **1989**, *179*, 124–
819 126.
- 820 (52) Reuillard, B.; Le Goff, A.; Agnès, C.; Holzinger, M.; Zebda, A.;
821 Gondran, C.; Elouarzaki, K.; Cosnier, S. *Phys. Chem. Chem. Phys.* **2013**,
822 *15*, 4892–4896.